Pergamon

Int. J. Solids Structures Vol. 33, No. 24, pp. 3561–3575, 1996

0020–7683/96 $15.00 + .00

0020–7683(95)00192–1

A PHENOMENOLOGICAL MODEL FOR PERFORATION OF MODERATELY THICK PLATES BY TUMBLING PROJECTILES

KEZHUN LI and WERNER GOLDSMITH
Department of Mechanical Engineering, University of California, Berkeley, CA 94720, U.S.A.

(*Received* 1 *February* 1995; *in revised form* 1 *August* 1995)

Abstract—A phenomenological model has been developed to describe the mechanism of tumbling perforation of blunt-faced cylindrical projectiles in moderately thick aluminum plates. The perforation process, based on experimental observations, consists of four stages: erosion; plugging; hole enlargement and petaling. The modeling in the plugging stage consists sequentially of cratering, plug formation, plug separation, plug slipping and post perforation deformation. Bulging and voids in the target created by projectile rotation were also considered in the model. The target material is considered to be rigid-perfectly plastic, while the projectile is regarded as undeformable. Calculations for the final velocity and oblique angle of the projectile as well as for the crater profile of the target were found to be in good correspondence with experimental results. Copyright © 1996 Elsevier Science Ltd.

NOTATION

A	projectile frontal surface area
c_p	compressive plastic wave speed in target
D	projectile diameter
F_f	force acting on projectile frontal surface
F_l	force acting on projectile lateral surface
H	target thickness
h	effective thickness of target
I_p	projectile moment of inertia
L	projectile length
m_p	projectile mass
M	total moment acting on projectile
M_f	moment acting on projectile frontal surface
M_l	moment acting on projectile lateral surface
p	indentation pressure
R	projectile radius
v	velocity of the projectile
v_q	final velocity of plug
X, Y, Z	coordinates
y_c	projectile center coordinate in Y direction
z_c	projectile center coordinate in Z direction
α	yaw angle
β	oblique angle
β_q	final oblique angle of plug
θ	impact angle
ρ_p	mass density of projectile
ρ_t	mass density of target
σ_y	dynamic yield stress of target material
σ_{yc}	dynamic constrained uniaxial yield stress
τ_y	dynamic shear stress
ω	rotational speed of projectile

INTRODUCTION

In penetration mechanics, most of the previous investigations have been concerned with normal impact of projectiles on stationary targets, where the velocity vector of the projectile is parallel to its axis of symmetry and normal to the plane of the target. The models given by Recht and Ipson (1963), Awerbuch and Bodner (1974), Liss and Goldsmith (1983) and

Yuan *et al.* (1983) are typical. To the authors' knowledge, investigations of tumbling penetration with combined yaw and obliquity are infrequent compared to normal impact though a certain amount of effort has been devoted to oblique impact (see e.g. Goldsmith and Cunningham, 1956; Zaid and Paul, 1959; Backman *et al.*, 1977; Awerbuch and Bodner, 1977; Goldsmith and Finnegan, 1986; Woodward and Baldwin, 1979), yaw impact (see e.g. Bless *et al.*, 1978; Hohler and Stilp, 1986; Cagliostro *et al.*, 1990; Bjerke *et al.*, 1992; Goldsmith *et al.*, 1995) or both (see e.g. Roecker and Grabarek, 1986). There are several reasons for this, one being the difficulty encountered in controlling this type of impact. In addition, the mechanism of the penetration process is very complicated due to its non-axisymmetric property. The nomenclature adopted in tumbling penetration is shown in Fig. 1. The yaw angle, α, is defined as the angle between the longitudinal axis of the projectile and the velocity vector of the projectile's center of mass. The oblique angle, β, is the angle between the velocity vector and the target normal. The impact angle, θ, is the angle between the projectile axis and the normal to the target so that $\theta = \alpha - \beta$.

The importance of tumbling impact lies in wide applications in military and civilian areas. Explosively-launched rods tumble and strike targets with a wide range of yaw angles. In oblique impact into multiple plates, the first layer deflects and rotates the projectile so that the projectile does not strike the targets normally or without rotation subsequently. Tumbling impacts may come from failure of high-speed rotors or high-speed rotating blades in any type of machinery such as an aircraft engine. The impact angle (or yaw angle with a zero oblique angle) due to tumbling can substantially reduce the penetration capability of the strikers. On the other hand, tumbling impact can cause larger crater sizes and change the trajectory of the projectile once perforations occur and thus may cause more damage than normal perforations. A quantitative analysis of this aspect is important in both armor and machinery design.

An experimental study by Li and Goldsmith (1996) concerned the impact response of moderately thick 6061-T6 aluminum plates ($H = 12.7$ mm) by tumbling cylindrical projectiles. This projectile motion was produced by overlapping contact of the plane-faced projectile with the edge of a generator placed between the gun and the target plate. The projectiles consisted of 12.7 mm diameter cylinders with an aspect ratio of 3 fired from a powder gun at speeds ranging from 300 to 650 m/s. The impact angles varied from 0° to 50°. Particular emphasis in the experimental study was placed on observations of the velocity and obliquity of the projectile after perforation.

In this paper, a phenomenological model was created on the basis of experimental observation of the major observed deformation features. The modeling requires reasonable assumptions during perforation such as consecutive stages. The perforation process was

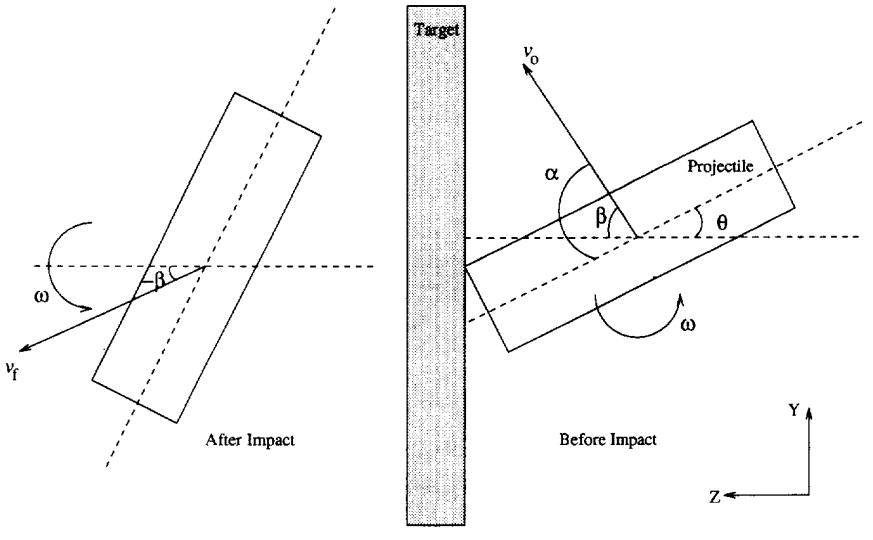

Fig. 1. Nomenclature relating to impact by a tumbling cylindrical projectile on plates.

modeled using combined momentum and energy approaches. A computer program was generated to evaluate the model. Results obtained provide the final translational velocity and oblique angle of the projectile and of the plug, as well as the crater profile of the targets. Comparisons of the experimental data and the analytical results were also performed.

PERFORATION MODEL FOR TARGETS OF INTERMEDIATE THICKNESS

The properties of the projectile and target are listed in Table 1, where the dynamic properties of the aluminum is taken from the paper by Awerbuch and Bodner, 1974. Based on the experimental observations, the penetration process in the present moderately thick targets (target thickness/projectile diameter = 1, which falls in the moderate range) can be characterized by four consecutive stages:

(i) erosion
(ii) plugging
(iii) hole enlargement
(iv) petaling.

A schematic representing a perforation process by a tumbling projectile in moderately thick aluminum targets is shown in Figs 2a–d. It was observed that the petaling stage will not materialize until the impact angle exceeds 25°. The target material is characterized as rigid-perfectly plastic, while the projectile is considered undeformable due to its high strength and hardness. Since the global deflection of the plate is very small, it is neglected in the analysis. Here, the case will be described where the impact angle is relatively small (less than 25°) so that no petaling is involved.

Erosion stage

Due to the impact angle, the projectile initially contacts the target at a point, when the first stage, erosion, commences. This stage continues until the entire face of the projectile has made contact with the plate. As a result of the relatively shallow impact angle, the penetration depth during this stage is small. This process is similar to those studied by Rickerby and MacMillan (1980) and Hutchings (1977, 1981). In such a case, the assumption of a uniform constant indentation pressure acting normal to the contact area for the oblique and yaw impact is appropriate; predictions using this value have compared well with corresponding experimental data. In the present investigation, the pressure is assumed to be equal to the indentation pressure or thrice the value of the yield stress of the target material (Bishop *et al.*, 1945), i.e.

$$p = 3.0\sigma_y \tag{1}$$

where p is the indentation pressure and σ_y the yield stress. The frictional force was found to be small (coefficient of friction is 0.05) by Rickerby and MacMillan (1980) and is therefore neglected in the current study. Also no account was taken of inertial effects in this stage.

The geometry of this phase is presented in Figs 3a–c. Figure 3a depicts the projectile of radius R and length L which has penetrated a target to a depth z_p. Figure 3b shows the projection of the frontal surface of the projectile. A cross-section of the cylinder at a distance x from the frontal surface of the projectile is shown in Fig. 3c. From Figs 3a and 3b, the force and the moment acting on the frontal surface of the projectile are:

Table 1. Properties of projectile and target materials

Material	Density ρ kg/m^3	Dynamic yield strength σ_y, MPa	Dynamic shear strength τ_y, MPa
Projectile	7977	1393	804
AL 6061	2780	295	190

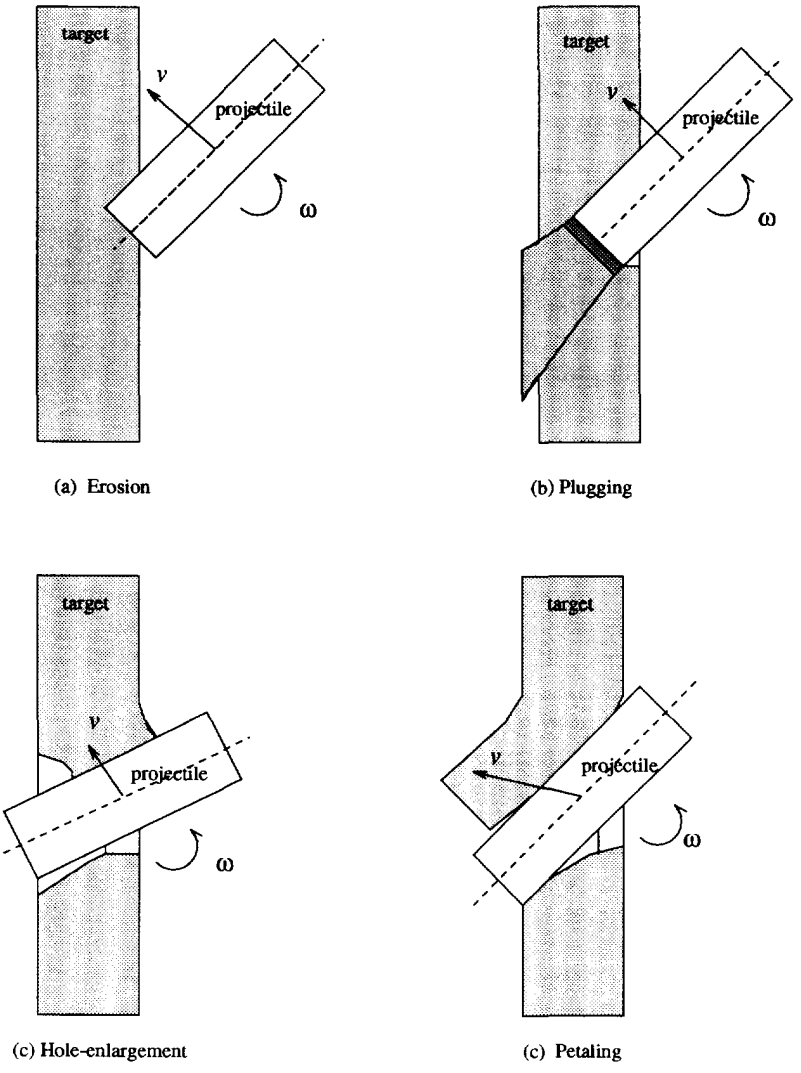

Fig. 2. Schematic of a perforation process by a tumbling cylindrical projectile on thick plates.

$$F_f = \int_{R-h}^{R} \mathrm{d}x_2 \int_{-\sqrt{R^2-x_2^2}}^{\sqrt{R^2-x_2^2}} p \, \mathrm{d}x_1 \tag{2}$$

$$M_f = \int_{R-h}^{R} \mathrm{d}x_2 \int_{-\sqrt{R^2-x_2^2}}^{\sqrt{R^2-x_2^2}} p x_2 \, \mathrm{d}x_1 \tag{3}$$

where

$$h = \frac{z_p}{\sin\theta} \tag{4}$$

$$z_p = z_c + \frac{L}{2}\cos\theta + R\sin\theta \tag{5}$$

and z_c is the coordinate of the center of the projectile C, as shown in the figure.

After integration of eqns (2) and (3), we have

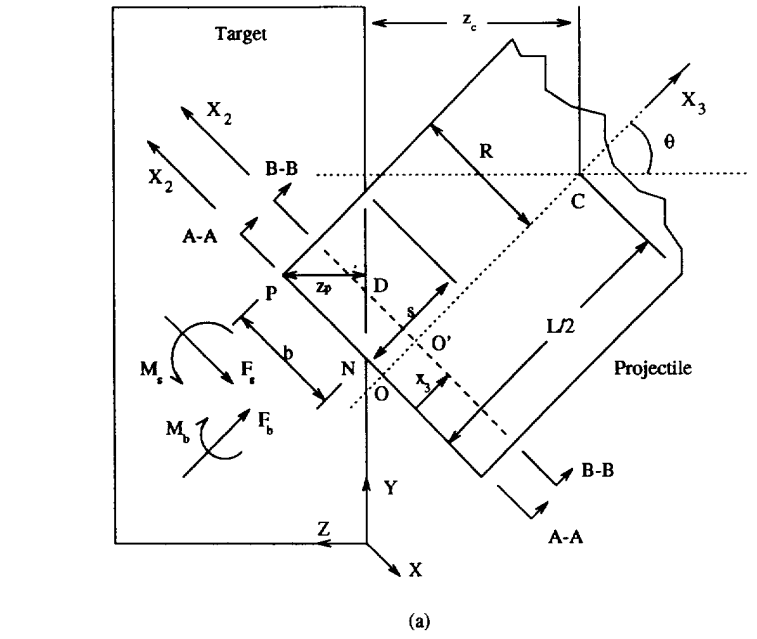

(a)

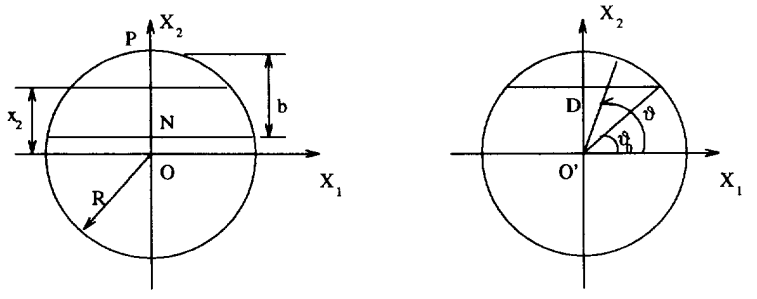

(b) A-A (c) B-B

Fig. 3. Projectile/target geometry during erosion stage for thick plates.

$$F_f = R^2 p\left[\frac{\pi}{2} - \sin^{-1}\frac{R-b}{R} - \frac{(R-b)\sqrt{2Rb-b^2}}{R^2}\right] \tag{6}$$

$$M_f = \tfrac{2}{3}p(2Rb-b^2)^{3/2} \tag{7}$$

From Figs 3a and 3c, the force and the moment from the lateral surface of the projectile are:

$$F_l = 2\int_0^s \mathrm{d}x_3 \int_{\vartheta_0}^{\pi/2} Rp\sin\vartheta\,\mathrm{d}\vartheta \tag{8}$$

$$M_l = 2\int_0^s \mathrm{d}x_3 \int_{\vartheta_0}^{\pi/2} Rp\left(\frac{L}{2}-x_3\right)\sin\vartheta\,\mathrm{d}\vartheta \tag{9}$$

where

$$s = \frac{z_p}{\cos\theta} \tag{10}$$

$$\vartheta_0 = \sin^{-1}\frac{O'D}{R} \tag{11}$$

and

$$O'D = R - \frac{s - x_3}{\tan\theta} \tag{12}$$

Thus

$$\vartheta_0 = \sin^{-1}\frac{R - (s - x_3)/\tan\theta}{R} \tag{13}$$

Integration of eqns (8) and (9) provides the relations

$$F_l = p\tan\theta\left[\frac{\pi R^2}{2} - \frac{R\sin\theta - z_p}{\sin^2\theta}\sqrt{z_p^2 - 2Rz_p\sin\theta} - R^2\sin^{-1}\left(1 - \frac{z_p}{R\sin\theta}\right)\right] \tag{14}$$

$$M_l = \left(\frac{L}{2} + R\tan\theta - \frac{z_p}{\cos\theta}\right)F_l - \tfrac{2}{3}p\tan^2\theta\left[R^2 - \left(R - \frac{z_p}{\sin\theta}\right)^2\right]^{3/2} \tag{15}$$

An exceptional case of impact with tumbling is normal impact where the projectile is in initial contact with the target over its entire face. For this situation, the erosion stage does not exist. Thus, the penetration begins with the plugging stage.

Plugging stage

Once the entire face of the projectile contacts the target, the second stage—plugging—will initiate. As in perforation at normal incidence, this stage consists of cratering, plug formation, plug separation, plug slipping and post-perforation deformation. A detailed description of all these processes can be found in the paper by Liss and Goldsmith (1983). Here, Liss's equations are modified to account for oblique position of the projectile due to tumbling. A representation of the plugging stage during tumbling perforation is shown in Figs 4a–d. From experimental observation, the bending effects for 12.7 mm thick plates were found to be small and are neglected in the present model. This assumption is also justified by the previous analysis (Jenq *et al.*, 1988) where, for the same projectile and target type, bending effects were reduced substantially when the plate thickness increased from 3.2 mm to 6.4 mm.

In tumbling penetration, the projectile moves both axially and laterally, and is further subjected to rotation. Forces act both on the frontal surface and on the lateral surface of the projectile. The forces acting on the frontal surface could still be derived from the case of normal perforation; however, since the projectile rotates, the effective thickness of the plate ($H/\cos\theta$) also changes. The plug is accelerated by the force from the frontal surface of the projectile. The lateral surface of the projectile is still acted upon by a pressure which is equivalent to the indentation pressure in the erosion stage. The plugging stage will end once the plug is completely ejected from the target plate. Figures 4a and 4b show the assumed geometry, axial displacements x_1, x_2, x_3, x_4 and velocities v_1, v_2, v_3, v_4 imparted to the surrounding target during penetration. The regions labeled 1, 2, 3, and 4 represent the projectile, the deformed plug portion, the outer target zone, and the undeformed part of the plug ahead of the projectile; zones 1, 2 and 4 move with uniform velocity. From Fig. 4, we have

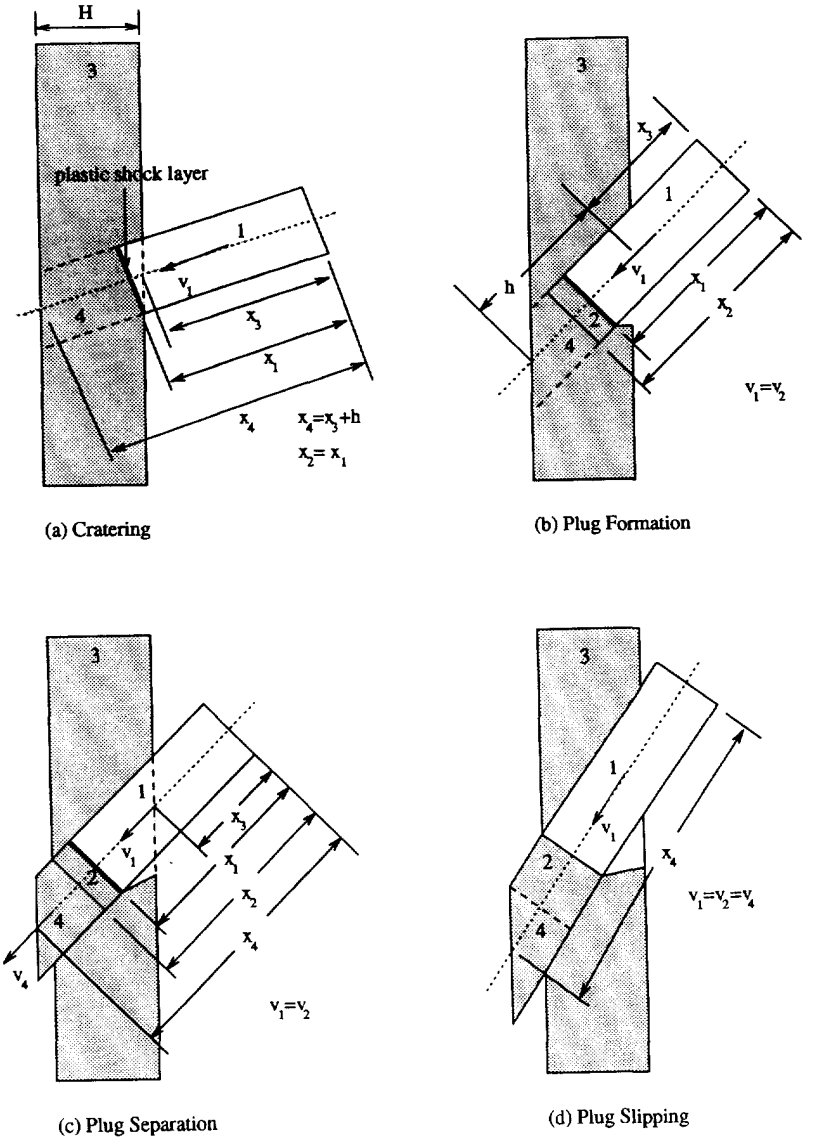

Fig. 4. Projectile/target geometry during plugging stage.

$$r_i = \dot{y}_c \cos\theta - \dot{z}_c \sin\theta \tag{16}$$

The mechanisms involved in the plugging include:

(1) sideways erosion (cratering) of material passing through the shock layer produced just ahead of the projectile-target interface when the relative velocity exceeds the plastic shock wave velocity in the target. The radial momentum of this plug section is imparted to the outer target zone;
(2) axial plastic wave propagation in the target zone ahead of the projectile. The shock wave has negligible thickness and material passing through this front is plastically deformed and instantaneously acquires the projectile velocity;
(3) material not yet reached by the plastic shock wave or that behind it acts as a rigid body, equivalent to the neglect of elastic strains;
(4) a constant value of the peripheral shear is assumed in a narrow annulus at the projectile boundary representing the adiabatic shear zone across which the velocity field is considered to exhibit a discontinuity.

The sequence of events is as follows.

Cratering. This occurs when the relative velocity of projectile and target exceeds the plastic wave speed of the target c_p which is given by (Liss and Goldsmith, 1983):

$$c_p = \frac{\sigma_{yc} - \sigma_y}{\rho_t v_1} \tag{17}$$

where σ_{yc} is the constrained uniaxial yield stress, $\sigma_{yc} = 1.97\sigma_y$ (Zukas, 1990); ρ_t is the target density. The thrust on the frontal surface of the projectile F_f is:

$$F_f = (\sigma_{yc} + \rho_t v_1^2)A \tag{18}$$

where A is the area of the face of the projectile, $A = \pi R^2$. This stage terminates when v_1 falls below c_p initiating plug formation.

Plug formation. The motion of the shock front divides the plug into rigid body regions moving with velocity $v_4 = 0$ and $v_2 = v_1$, as shown in Fig. 4b; the decreasing mass m_4 remains unmoved while increasing mass m_2 moves with the projectile speed v_1. The force F_f during this stage is given by

$$F_f = \frac{[\sigma_{yc}A + 2\pi R\tau_s(x_2 - x_1)]m_p}{m_p + \rho_t A(x_2 - x_1)} \tag{19}$$

where τ_s is the dynamic shear stress at the periphery. Termination of this stage occurs when the force applied by the shock front is about to exceed the maximum resistive peripheral shear force, or

$$\sigma_{yc}A = 2\pi R\tau_s(x_3 + h - x_2) \tag{20}$$

where h is the effective thickness given by $h = H/\cos\theta$.

Plug separation from the rear target face. This stage, shown in Fig. 4c, terminates when either the complete plug attains projectile velocity v_1 before completion of physical separation from the target, or when detachment of the rear plug face from the distal target surface occurs before the plug attains v_1 (perforation). The force F_f during this stage, composed of lateral momentum transfer and peripheral shear, is given by:

$$F_f = \sigma_{yc}A + v_1(v_1 - v_4)A\rho_t + 2\pi R\tau_s(x_4 - x_1). \tag{21}$$

Plug slipping. This stage, shown in Fig. 4d, starts when the complete plug, nearly excised, is assumed to slip with constant velocity $v_4 = v_2 = v_1$ opposed only by peripheral plastic shear, friction being neglected. The force on the frontal surface of the projectile is given by

$$F_f = \frac{2\pi R\tau_s(h + x_3 - x_1)}{m_p + \rho_t A(x_4 - x_1)}m_p. \tag{22}$$

Post perforation deformation. This occurs if the plug has been completely separated before acquiring projectile velocity. Erosion and shock wave propagation may occur successively without either constraint to side flow or peripheral shear action. For shock wave propagation, the force is given by

$$F_f = \sigma_y A \frac{m_p}{m_p + \rho_t A(x_2 - x_1)}. \tag{23}$$

Arrest of the shock wave occurs when the velocity of element 4 attains that of region 1.

Hole enlargement stage

Once the plug is completely ejected from the target, the hole enlargement stage is initiated. Since the ratio of the target thickness to the diameter of the projectile is greater than 1 (using the "effective" target thickness here, as described above), the state of the plate lies somewhere between plane strain and plane stress, since the above ratio is reduced due to the bulging effect (as will be shown later). However, a plane strain case is assumed for simplicity. For such a situation, the pressure due to symmetric hole enlargement consists of two parts, a static and a dynamic component. Generally, the dynamic pressure is proportional to the square of the normal velocity component on the lateral surface of the projectile. Due to the assumed relatively small impact and oblique angles, the normal velocity component is small and so is the dynamic pressure which, hence, is neglected here. When using these parameters, it should be noted that the hole enlargement process in the present case is different from that of the axisymmetric case that occurs for thin plates. The static pressure can still be regarded as evenly distributed along the edge of the hole and equal to that for an axisymmetric penetration situation, so that

$$p = k\sigma_y \tag{24}$$

where $k = 3$ for a plane strain condition.

It was observed that the material around the edge of the hole piled up appreciably due to hole enlargement, which resulted in thickening around the edge and produced an additional contact area between the target and the lateral surface of the projectile. In the present model, the contact area is still not considered to have experienced thickening—a condition believed to be justified below. Due to the assumption of plane strain, the pressure p for this non-plane strain case is overestimated. It is believed that the effect of thickening is compensated by an increase of pressure given by eqn (24) on the contact area. This stage will terminate when the projectile loses contact with the target completely or when petaling begins.

Petaling stage

Cracks are assumed to be produced once the plug is ejected from the target. The contact pressure acting on the projectile will accelerate its rotation and thus increase the impact angle. When the impact angle reaches a certain value, the tearing force will become large enough to initiate crack propagation and cause petaling. From experimental observation, the critical impact angle was found to be around 25° for 12.7 mm thick 6061-T6 aluminum plates. This stage may occur when the impact angle gets to the critical value during the hole enlargement or when the impact angle already exceeds the critical value before the hole enlargement. The energy dissipated during this process includes mainly plastic deformation that accounts for the projectile and the petal reaching a common velocity, extension of existing cracks, and change in momentum of the petals. This stage is not considered in the current model.

Consideration of voids

In penetration with tumbling, the projectile experiences not only translational motion, but also rotation. This may produce voids in sections of the target previously indented, but

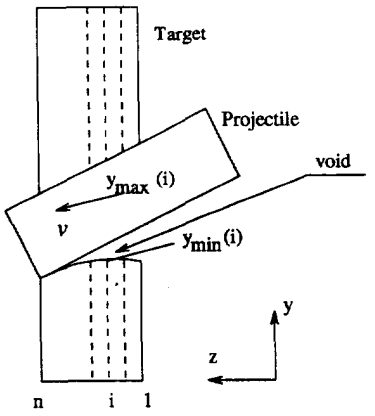

Fig. 5. Description of voids and contour of target deformation.

vacated by projectile rotation as shown in Fig. 5. In such cases, the pressure in this section is zero. Also, when the normal velocity of the projectile at some point is directed inward rather than outward, i.e. that point is moving away from the target crater edge, the pressure must be equal to zero at this point. To address this situation, the entire lateral surface of the projectile is divided into smaller elements, and these elements are fixed in the projectile and do not change with time. At every instant, each element of the projectile is checked to see if it is in contact with the target or not. The normal velocity at each element (in fact, the element center) is also checked. If the element of the projectile is in contact with the target and the normal velocity is directed outward, there is pressure; otherwise, the pressure is set equal to zero. In order to determine if the element of the projectile is in contact with the target, the deformation contour of the target at each instant needs to be obtained. Numerically, this is done by choosing a certain number of points fixed in the target, $i = 1, 2, \ldots, n$, as shown in Fig. 5. Corresponding to each point $z(i)$, the extremes of the contour can be represented by two values, $y_{min}(i)$ and $y_{max}(i)$. At each time, the corresponding point on the boundary of the projectile is checked. If it is within the area bounded by $y_{min}(i)$ and $y_{max}(i)$, then the values representing the contour at this point, i.e. $y_{min}(i)$ and $y_{max}(i)$ remain unchanged. If the point is either below $y_{min}(i)$ or above $y_{max}(i)$, then this point will replace $y_{min}(i)$ or $y_{max}(i)$, and an enlarged area is formed. The region between $y_{min}(i)$ and $y_{min}(i+1)$ or $y_{max}(i)$ and $y_{max}(i+1)$ is represented by a linear interpolation of the two points, i.e.

$$y_{min}(z) = y_{min}(i) + \frac{y_{min}(i+1) - y_{min}(i)}{z(i+1) - z(i)}[z - z(i)] \tag{25}$$

$$y_{max}(z) = y_{max}(i) + \frac{y_{max}(i+1) - y_{max}(i)}{z(i+1) - z(i)}[z - z(i)] \tag{26}$$

The advantage of using this technique is that once the penetration terminates, the contour, or the crater profile, has been determined.

Bulging effect

Bulging effects were observed in both normal and tumbling perforations; this phenomenon is shown schematically in Fig. 6. The diameter of the cavity was found to increase appreciably towards the exit. This will change the real contact area of the target/projectile lateral surface. Even though in Liss and Goldsmith' model for normal perforation (1983), the effect of bulging was not considered, i.e. the plug was treated as a uniform cylinder with the same diameter as that of the projectile, that model gives good results (as will be shown later). The reason is that there is no contact pressure between the target and the projectile lateral surface in the normal perforation model so that the effect of bulging, or change of the cavity does not have an effect on the projectile motion. In tumbling perforation,

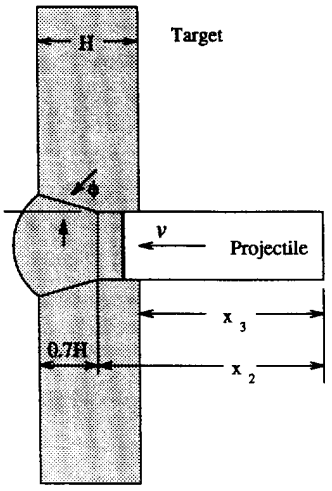

Fig. 6. Description of bulging effect in perforation.

however, bulging will have a significant effect on the actual contact area of the target/projectile. This will affect the force acting on the projectile lateral surface during the hole enlargement stage and subsequently the motion of the projectile. Hence, bulging is important and can not be neglected.

Examination of the specimens showed that the cavity diameter increases linearly with depth starting at about $0.7H$ from the distal side. This value is close to the one (0.66–0.85) found in perforation of a porous medium (Ross, 1968). The angle ϕ shown in Fig. 6 is nearly 15° in all normal and tumbling perforations. In the present model, the bulging effect is considered in the third stage, i.e. plug separation from the rear target face. When the thrust applied by the shock front is about to exceed the maximum resistive peripheral shear force, the plug will separate along the lines shown in the figure. At this moment, from eqn (20) and Fig. 4b, we have

$$x_3 + h - x_2 = \frac{\sigma_{3c} A}{2\pi R \tau_s} \tag{27}$$

Using the properties of 12.7 mm thick 6061-T6 aluminum targets listed in Table 1, the starting point of the bulge is:

$$x_3 + h - x_2 = 0.78H \tag{28}$$

which is close to the experimental value.

Equation of motion of the projectile

Once the forces and the moments from both the face and lateral surface of the projectile have been determined, the equations of motion of the projectile can be derived from Newton's second law.

The equations of motion of the projectile are:

$$F_z = m_p \ddot{z}_c \tag{29}$$

$$F_y = m_p \ddot{y}_c \tag{30}$$

$$M = I_p \ddot{\theta} \tag{31}$$

where F_z and F_y are the force components, M is the moment, and I_p is the moment of inertia of the projectile, with

$$m_p = \pi R^2 L \rho_p \tag{32}$$

$$I_p = m_p\left[\frac{R^2}{4} + \frac{L^2}{12}\right] \tag{33}$$

with initial conditions:

$$\theta(0) = \theta_0 \tag{34}$$

$$\dot{z}_c(0) = v_0 \cos\beta_0 \tag{35}$$

$$\dot{y}_c(0) = v_0 \sin\beta_0 \tag{36}$$

$$\dot{\theta}(0) = \omega_0 \tag{37}$$

From Fig. 3a, we have:

$$F_z = -F_f\cos\theta - F_l\sin\theta \tag{38}$$

$$F_y = F_f\sin\theta - F_l\cos\theta \tag{39}$$

$$M = M_l - M_f \tag{40}$$

The equations of motion of the projectile were numerically integrated using a step-by-step Euler finite difference method: the new position and orientation of the projectile after an additional time increment were computed and the process repeated.

RESULTS AND DISCUSSION

The phenomenological model developed above has been programmed in FORTRAN language and calculated numerically. The program input data include material constants, problem geometry, and kinematic parameters of the projectile. The computational output provides predictions of the final velocity and oblique angle of the projectile and the plug as well as the crater profile in the target.

Simulations of 15 runs for 12.7 mm thick 6061-T6 aluminum plates, two of which were normal perforations, were performed based on the analytical model indicated above. The computational results and the corresponding experimental data are presented in Table 2.

Table 2. Experimental and analytical results of perforation of plates by tumbling projectiles

	Initial conditions				Final result							
					Experimental				Analytical			
	projectile				projectile		plug		projectile		plug	
Run	v_0 m/s	θ_0 deg	β_0 deg	ω_0 rad/s	v_f m/s	β_f deg	v_q m/s	β_q deg	v_f m/s	β_f deg	v_q m/s	β_q deg
T1	404	17.8	−4.8	1075	253	−40.4	346	1.5	287	−41.7	299	−26.9
T2	339	9.0	12.1	74	172	−40.5	217	−22.5	186	−50.8	215	−19.7
T3	523	10.9	6.8	659	381	−24.9	426	−4.2	372	−28.2	406	−16.2
T4	476	12.3	−3.4	387	361	−25.2	411	1.5	378	−24.1	387	−16.6
T5	505	6.6	4.6	1674	395	−19.4	410	−8.2	378	−23.8	404	−12.9
T6	620	8.7	4.6	2264	478	−20.7	505	−11.2	463	−18.9	501	−14.4
T7	630	9.2	1.1	678	530	−15.0	556	−6.7	516	−18.0	527	−12.1
T8	562	10.2	3.7	1591	413	−21.3	474	−5.8	416	−25.0	447	−15.9
T9	438	21.6	7.8	1975	218	−43.2	—	—	179	−55.9	233	−40.1
T10	515	0.0	3.8	−80	421	−9.5	457	−4.7	429	−2.0	430	−0.6
T11	372	0.6	6.8	78	266	−12.6	302	−0.6	281	−11.8	286	−3.1
T12	635	2.3	2.9	517	551	−7.4	554	−1.6	540	−6.2	543	−3.8
T13	536	18.5	7.2	1095	332	−27.3	—	—	324	−29.8	401	−15.5
T14	565	0.0	0.0	0	478	0.0	514	0.0	478	0.0	478	0.0
T15	402	0.0	0.0	0	323	0.0	349	0.0	320	0.0	320	0.0

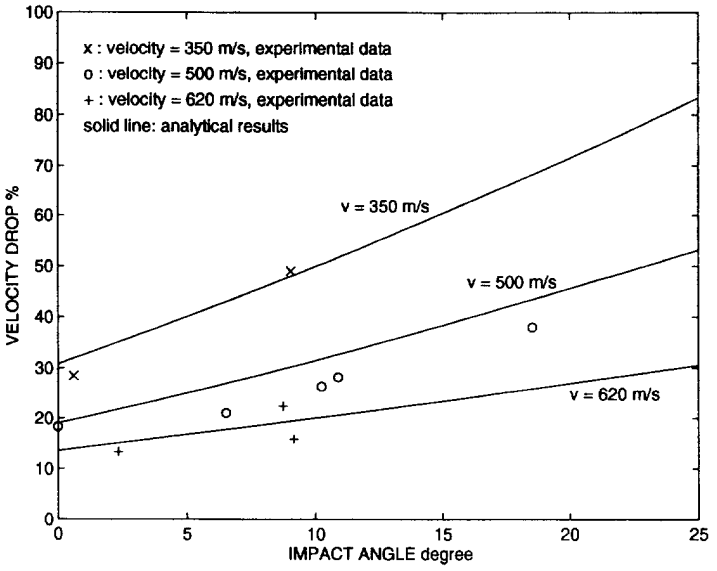

Fig. 7. Experimental and analytical results of velocity drop as a function of impact angle for 12.7 mm thick 6061-T6 aluminum plates struck by hard-steel blunt-faced cylindrical projectiles. Initial oblique angle is 5°.

Good correlation was found both in the final velocity and the final oblique angle of the projectile. The computed and the measured final velocities of the plug are in satisfactory agreement, but the oblique angles are not. The following discussion will focus on the velocity drop $(v_0 - v_f)/v_0$ and final oblique angle of the projectile as functions of the impact angle and initial velocity. The average initial oblique angle of all the runs is around 5°. As shown by Li and Goldsmith (1996), the effect of the initial rotational speed on the perforation process is small for the range presently investigated; therefore, it was neglected in the discussion. However, the major role of the rotation is to change the impact angle of the projectile at contact, and this will significantly affect the perforation process. Figures 7 and 8 show the velocity drop and final oblique angle of the projectile as a function of the impact angle for given initial velocities of 350, 500 and 620 m/s. It is seen that the velocity drop increases with impact angle and decreases with initial translational velocity. The absolute

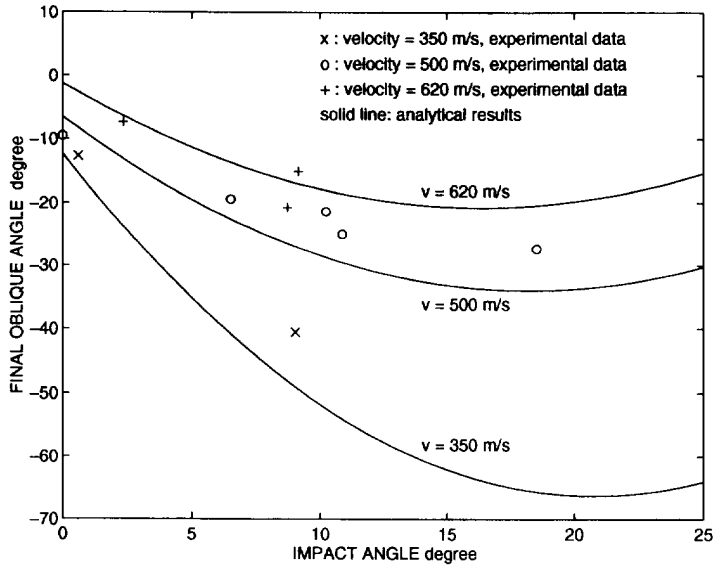

Fig. 8. Experimental and analytical results of final oblique angle as a function of impact angle for 12.7 mm thick 6061-T6 aluminum plates struck by hard-steel blunt-faced cylindrical projectiles. Initial oblique angle is 5°.

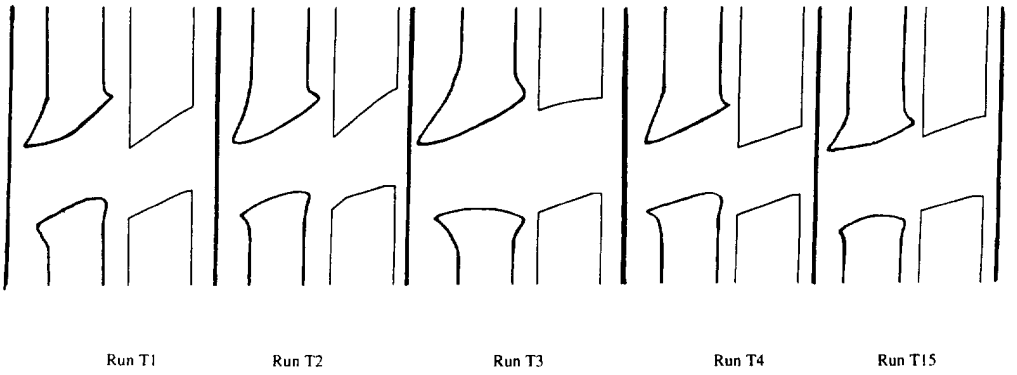

Fig. 9. Cross section of crater profiles for 12.7 mm thick 6061-T6 aluminum formed by tumbling perforation. Left: experimental data. Right: analytical prediction.

value of the final oblique angle increases with increasing impact angle when the impact angle is below a certain value (22° for 350 m/s; 18° for 500 m/s; and 15° for 620 m/s), but decreases when the impact angle is above this limit. A higher initial velocity reduces the magnitude of the final oblique angle, as shown in Fig. 8. Figure 9 presents the comparison of some of the calculated and measured cross-sectional crater profiles, and reasonable agreement was obtained.

For normal perforations such as runs T14 and T15, the model was the same as the wave propagation model presented by Liss and Goldsmith (1983). It is seen from Table 2 that this model gave excellent correspondence with the experimental data.

In general, the velocity drop predicted by the analytical model correlated very well with the experimental data when the impact angle was small, but was overestimated when the impact angle increased. The same phenomena were observed in the absolute value of the final oblique angle of the projectile. This can be explained as follows: with an increase of the impact angle, the failure mode tends to be petaling rather than hole-enlargement because petaling consumes less energy under these conditions according to the minimum potential energy principle. However, in the current model, hole enlargement is assumed to dominate the penetration process after the plugging stage. Thus, prescribing hole enlargement in such a situation will lead to more energy dissipation, or, in other words, larger resisting forces acting on the projectile. This, in turn, results in a higher velocity drop and an increase in the absolute value of the final oblique angle. The final velocities of the plug predicted by the analytical model were close to those found in the experiments but were underestimated in most of the runs. The oblique angle of the plugs in the experiments showed irregular distribution and did not correlate with the impact angle and the initial velocity. The same phenomenon was also observed by Woodward (1979). Due to oblique position of the projectile during the perforations, forces acting on the plugs are not axi-symmetric and direction of the plug is strongly affected by the last portion of shear process, which is hard to predict. This makes the motion of the plugs very complicated.

CONCLUSION

A phenomenological model was constructed to analyze the perforation of moderately thick aluminum plates by tumbling, blunt-faced hard-steel cylindrical projectiles. This model was based on experimental observations that indicated the presence of four consecutive stages: erosion, plugging, hole enlargement and petaling. The petaling, which occurs when the impact angle is above 25°, is not considered in the current model. Bulging and void effects were also considered in the model. Calculations for the system response were performed for 15 impact configurations including those corresponding to test results described elsewhere (Li and Goldsmith, 1996). Such data, obtained for the final velocity and final oblique angle of the projectile as well as the crater profile produced in the targets, were compared with corresponding model predictions.

It was found that increasing the impact angle results in a noticeable increase of the velocity drop of the projectile, as expected *a priori*. The final oblique angle of the projectile increases substantially at first, but decreases rapidly to zero with further increase of the impact angle. Higher velocity tends to reduce the velocity drop and change of the final oblique angle.

The phenomenological model predicts the final velocity and oblique angle of the projectile quite well when the impact angle is small (below 25°). With an increase of the impact angle, the model overestimates the velocity drop and the absolute value of the final oblique angle. In such a case, the petaling dominates the failure mode of the target instead of the hole enlargement and should be incorporated in the model.

Acknowledgement—This work constitutes a portion of a doctoral dissertation by the first author at the University of California, Berkeley. The work was sponsored by the Air Force Office of Scientific Research, Bolling Air Force Base, Washington, D.C., under contract AFOSR F49620-89-8127.

REFERENCES

Awerbuch, J. and Bodner, S. R. (1974). Analysis of the mechanics of perforation of projectiles in metallic plates. *Int. J. Solids & Struct.* **10,** 671–684.

Awerbuch, J. and Bodner, S. R. (1977). An investigation of oblique perforation of metallic plates by projectiles. *Exp. Mech.* **17,** 147–153.

Backman, M. E., Finnegan, S. A. and Whitman, K. G. (1977). Dynamics of the oblique impact and ricochet of nondeforming projectiles against thin plates. In *Recent Advances in Engineering Science*, (ed. G. C. Sih) Lehigh University Publication, Bethlehem, PA, pp. 9–20.

Bishop, R. F., Hill, R. and Mott, N. F. (1945). The theory of indentation and hardness tests. *Proc. Phys. Soc.* **57,** 147–159.

Bjerke, T. W., Silsby, G. F., Scheffler, D. R. and Mudd, R. M. (1992). Yawed long-rod armor penetration. *Int. J. Impact Engng* **12,** 281–292.

Bless, S. J., Barber, J. P., Bertke, R. S. and Swift, H. F. (1978). Penetration mechanics of yawed rods. *Int. J. Engng Sci.* **16,** 829–834.

Cagliostro, D. J., Mandell, D. A., Schwalbe, L. A., Adams, T. F. and Chapyak, E. J. (1990). MESA 3-D calculations of armor penetration by projectiles with combined obliquity and yaw. *Int. J. Impact Engng* **10,** 81–92.

Goldsmith, W. and Cunningham, D. M. (1956). Kinematic phenomena observed during the oblique impact of a sphere on a beam. *J. Appl. Mech.* **23,** 612–616.

Goldsmith, W. and Finnegan, S. A. (1986). Normal and oblique impact of cylindro-conical and cylindrical projectiles on metallic plates. *Int. J. Impact Engng* **4,** 83–105.

Goldsmith, W., Tam, E. and Tomer, D. (1995). Yawing impact on thin plates by blunt projectiles. *Int. J. Impact Engng* **16,** 479–498.

Hohler, V. and Stilp, A. J. (1986). Influence of the primary yaw angle on the secondary yaw angle during armor plate perforation. *Proc. Sixth Int. Symp. Ballistics*. Orlando, Florida, 27–29 October 1981, pp. 302–308.

Hutchings, I. M. (1977). Deformation of metal surfaces by the oblique impact of square plates. *Int. J. Mech. Sci.* **19,** 45–52.

Hutchings, I. M. (1981). Further studies of the oblique impact of a hard sphere against a ductile solid. *Int. J. Mech. Sci.* **23,** 639–646.

Jenq, S. T., Goldsmith, W. and Kelly, J. M. (1988). Effect of target bending in normal impact of a flat-ended cylindrical projectile near the ballistic limit. *Int. J. Solids Struct.* **24,** 1243–1266.

Li, K. and Goldsmith, W. (1996). Impact on aluminum plates by tumbling projectiles: experimental study. *Int. J. Impact Engng* **18,** 23–43.

Liss, J., Goldsmith, W. and Kelly, J. M. (1983). A phenomenological penetration model of plates. *Int. J. Impact Engng* **1,** 321–341.

Recht, R. F. and Ipson, T. W. (1963). Ballistic perforation dynamics. *J. Appl. Mech.* **30,** 384–390.

Rickerby, D. G. and Macmillan, N. H. (1980). On the oblique impact of a rigid sphere against a rigid-plastic solid. *Int. J. Mech. Sci.* **22,** 491–494.

Roecker, E. and Grabarek, C. (1986). The effect of yaw and pitch on long rod penetration into rolled homogeneous armor at various obliquities. *Proc. Ninth Symp. Ballistics*. Shrivenham, UK, pp. 29–30.

Ross, Bernard (1968). The perforation of a porous medium due to projectile impact. *Experimental Mech.* **8,** 444–495.

Woodward, R. L. and Baldwin, N. J. (1979). Oblique perforation of targets by small armor-piercing projectiles. *J. Mech. Engng Sci.* **21,** 85–91.

Yuan, W., Zhou, L., Ma, X. and Stronge, W. (1983). Plate perforation by deformable projectiles—a plastic wave theory. *Int. J. Impact Engng* **1,** 393–412.

Zaid, M. and Paul, B. (1959). Oblique perforation of a thin plate by a truncated conical projectile. *J. Franklin Inst.* **268,** 25–45.

Zukas, J. A. (ed.) (1990). *High Velocity Impact Dynamics*, John Wiley, New York, pp. 1–64.